Salt-Dependent Compaction of Di- and Trinucleosomes Studied by Small-Angle Neutron Scattering

Markus Hammermann,* Katalin Tóth,* Claus Rodemer,* Waldemar Waldeck,* Roland P. May,† and Jörg Langowski*

*Division of Biophysics of Macromolecules, German Cancer Research Center, D-69120 Heidelberg, Germany, and †Institut Laue-Langevin Grenoble, F-38042 Grenoble, France

ABSTRACT Using small-angle neutron scattering (SANS), we have measured the salt-dependent static structure factor of di- and trinucleosomes from chicken erythrocytes and from COS-7 cells. We also determined the sedimentation coefficients of these dinucleosomes and dinucleosomes reconstituted on a 416-bp DNA containing two nucleosome positioning sequences of the 5S rDNA of *Lytechinus variegatus* at low and high salt concentrations. The internucleosomal distance *d* was calculated by simulation as well as Fourier back-transformation of the SANS curves and by hydrodynamic simulation of sedimentation coefficients. Nucleosome dimers from chicken erythrocyte chromatin show a decrease in *d* from ~220 Å at 5 mM NaCl to 150 Å at 100 mM NaCl. For dinucleosomes from COS-7 chromatin, *d* decreases from 180 Å at 5 mM to 140 Å at 100 mM NaCl concentration. Our measurements on trinucleosomes are compatible with a compaction through two different mechanisms, depending on the salt concentration. Between 0 and 20 mM NaCl, the internucleosomal distance between adjacent nucleosomes remains constant, whereas the angle of the DNA strands entering and leaving the central nucleosome decreases. Above 20 mM NaCl, the adjacent nucleosomes approach each other, similar to the compaction of dinucleosomes. The internucleosomal distance of 140–150 Å at 100 mM NaCl is in agreement with distances measured by scanning force microscopy and electron microscopy on long chromatin filaments.

INTRODUCTION

In the eukaryotic cell, chromatin is packaged into a fiber of 30 nm diameter (van Holde, 1989). The structure of this 30-nm fiber remains an enigma. More than 20 years ago, Finch and Klug proposed a simple helical model with about six nucleosomes per turn and 11 nm of fiber length (Finch and Klug, 1976). This solenoid model, or variants thereof, has been introduced into many textbooks; however, a number of studies have yielded evidence against the model (e.g., Rydberg et al., 1998; van Holde and Zlatanova, 1996; Zlatanova et al., 1998), and a large variety of alternative models have been proposed (reviewed in Woodcock and Horowitz, 1995; van Holde and Zlatanova, 1995, 1996; Widom, 1998). Recently, electron cryomicroscopy images indicated a structural motif of nucleosomes, linker DNA, and linker histones, leading to a zigzag structure both at low and high salt concentrations (Bednar et al., 1998). While the structure of the nucleosome core particle with 146 bp of DNA has been solved at a resolution of 2.8 Å (Luger et al., 1997), the question of whether the solenoid model is an adequate description has not yet been satisfactorily answered.

Because the histone octamer structure is conserved in all organisms and the diameter and the appearance of the 30-nm fiber are also very similar in most studies, it is widely believed that the higher order structure of the 30-nm fiber is universal. On the other hand, differences in the structure of the fiber between organisms might result from different DNA repeat lengths that range from 156 bp (Godde and Widom, 1992) to more than 240 bp (van Holde, 1989).

Most older models assume a regular structure of the fiber. Some studies based on newer techniques like scanning force or cryoelectron microscopy or, more recently, on a comparison of measured and simulated size distributions of DNA in chromatin after radiation damages, support a more random structure (Bednar et al., 1995; Woodcock and Horowitz, 1995; van Holde and Zlatanova, 1996; Rydberg et al., 1998). Some features of the fiber seem to be clear at this time. The linker histones play an important role in the folding process, and they are likely to be located in the interior of the 30-nm fiber (Graziano et al., 1994). The globular domain of the linker histones and the tails of histone H3 are required for the conformational stability of the fiber (Leuba et al., 1998a,b). The mass per unit length depends on the salt concentration and reaches a maximum value of six or seven nucleosomes per 11 nm at 100 mM NaCl (Gerchman and Ramakrishnan, 1987).

One criterion that might help to distinguish between the different models proposed for the 30-nm fiber is the extent to which the linker DNA between two adjacent nucleosomes can change its structure under different conditions (van Holde and Zlatanova, 1996). If it bends substantially, the solenoidal models would gain support, because a bent or curved linker is needed for side-by-side packing of adjacent nucleosomes. In his review, van Holde pointed out that most of the data indicate that the linker remains extended, even at

Received for publication 14 September 1999 and in final form 31 March 2000.

Address reprint requests to Dr. Jörg Langowski, Division of Biophysics of Macromolecules, German Cancer Research Center, Im Neuenheimer Feld 280, D-69120 Heidelberg, Germany. Tel.: 49-6221-423390; Fax: 49-6221-423391; E-mail: joerg.langowski@dkfz-heidelberg.de.

0006-3495/00/07/584/11 $2.00

elevated salt concentrations. The main contradiction arose from sedimentation data on rat liver dinucleosomes, which did not show any compaction (Butler and Thomas, 1980), and light scattering data on chicken erythrocyte dinucleosomes, which were found to compact with increasing salt (Yao et al., 1990), even without the linker histones (Yao et al., 1991). More recently, the dinucleosome sedimentation experiments were repeated with chicken erythrocyte dinucleosomes and an improved method of analysis (Butler and Thomas, 1998). The conclusion was well in line with the findings by Yao et al.: a salt-dependent compaction of chicken erythrocyte dinucleosomes with and without linker histones yielded support for bent linkers.

We decided to use a complementary approach. First, we measured the sedimentation coefficients of dinucleosomes from monkey kidney COS-7 cells (190-bp repeat length) and chicken erythrocyte chromatin (210-bp repeat length), both containing the linker histones, and reconstituted dinucleosomes lacking the linker histones, at low and high salt concentrations. Second, we simulated sedimentation coefficients by use of the program HYDRO (Garcia de la Torre et al., 1994) and compared them with our data and the measured data by Butler and Thomas to extract more quantitative information about the compaction process of di- and trinucleosomes. Third, we collected neutron scattering data on di- and trinucleosomes from COS-7 cells and from chicken erythrocytes, at salt concentrations between 5 and 100 mM NaCl. It was possible to determine the internucleosomal distances by simulation and Fourier back-transformation of the scattering curves. The data are compared with scanning force and cryoelectron microscopy images.

MATERIALS AND METHODS

Preparation of nuclei from chicken erythrocytes

Fresh chicken blood (5 ml) was washed twice with ice-cold Tris buffer (10 mM Tris-HCl, 100 mM NaCl, 1 mM EDTA, pH 7.5). After centrifugation at 2500 rpm in a Heraeus-Varifuge K centrifuge ($\sim$1200 $\times$ *g*), the erythrocyte pellet was resuspended in 50–60 ml reticulocyte standard buffer (RSB) (10 mM Tris-HCl, 10 mM NaCl, 3 mM $MgCl_2$, pH 7.4). Detergent NP40 (10%) was added to a final concentration of 0.5%. After several vortexing steps, interrupted by cooling on ice, the nuclei were pelleted at 2500 rpm in the Varifuge K centrifuge.

Preparation of nuclei from COS-7 cells

COS-7 cells were grown in tissue culture in RPMI 1640 medium supplemented with 10% fetal calf serum and 1% penicillin and streptomycin. Confluent monolayers in 15-cm Petri dishes were placed on ice and washed once with isotonic Tris-buffer (137 mM Tris-HCl, 5 mM KCl, 0.3 mM Na_2HPO_4, 0.5 mM $MgCl_2$, 0.7 mM $CaCl_2$, pH 7.5), followed by two washes with isotonic HEPES buffer (50 mM HEPES-NaOH, 220 mM sucrose, 1 mM EDTA, 1 mM dithiothreitol, pH 8.0). The cells were scraped from the dishes with a rubber policeman on ice into 50-ml polypropylene tubes (Falcon) and washed isotonically (as above) before the preparation of the nuclei. Detergent NP40 (10%) was added to a final concentration of 0.5%. The cells were vortexed for 90 sec and for 3 $\times$ 30 sec, interrupted by the same time intervals on ice. The nuclei were pelleted at 2000 rpm in a Heraeus Varifuge. The nuclear pellet was resuspended in RSB and 50% glycerol at a DNA concentration in the nuclei of $\sim$1 mg/ml and could be stored at -80°C.

Preparation of chromatin oligomers

The nuclear pellet was washed twice with 10 ml RSB and centrifuged as above. The nuclei were suspended in 50 ml RSB, which then contained $\sim$400–500 A_{260} units (18–20 mg DNA content). MNase digestion was performed with 1 unit MNase/ml. A $CaCl_2$ solution (final concentration 5 mM) was added, and the incubation time was 20 min at 37°C. The reaction was stopped by the addition of EGTA to a final concentration of 10 mM. The nuclei were then pelleted at 2500 rpm and resuspended in hypotonic 0.2 mM EDTA. Chicken erythrocyte and COS-7 chromatin oligomers were separated by centrifugation in at least two consecutive linear sucrose gradients (10–30%) underlayed with a 70% (1 ml) cushion in a Beckman SW41 rotor at 30.000 rpm for 20 h at 4°C, in Tris buffer (10 mM Tris, 100 mM NaCl, 1 mM EDTA, pH 7.5). After the first run the isolated fractions were combined and dialyzed in dialysis bags overnight against Tris buffer. The samples were concentrated before the second centrifugation step in Centricon cartridges (Centriprep 10, Centricon; Amicon, Beverly, MA). All chromatin samples were stored on wet ice. Aliquots of the fractions were analyzed for their DNA content after treatment with 1% sodium dodecyl sulfate (SDS) and 50 μg/ml proteinase K in 2% agarose gels stained with ethidium bromide (1 μg/ml). The protein content and the histone composition were analyzed in 18% polyacrylamide gels containing 0.1% SDS (29:1 acrylamide:bisacrylamide, 19 h, 3 V/cm). After electrophoresis the SDS was partially removed by rinsing the gel in electrophoresis buffer without SDS, followed by staining with Nile Red and photography under UV light; alternatively, the gel was stained by a standard Coomassie protein staining procedure. The samples were examined for the presence of free DNA or nucleosome sliding in 6% polyacrylamide gels (60:1 acrylamide:bisacrylamide, 0.09 M Tris, 0.09 M borate, 2 mM EDTA, pH 8.0, 3 h, 7 V/cm) before and after the sedimentation and the neutron scattering experiments. Some chromatin samples were concentrated in VivaSpin concentration tubes (VS0111 and VS0423; Vivascience, Lincoln, UK).

Dinucleosome reconstitution

A plasmid pBluescript (pBS) 5S-208-2 (3374 bp) containing two 208-bp nucleosome positioning sequences 5SrDNA from *Lytechinus variegatus* (Dong and van Holde, 1991) was cloned starting from plasmid pPolI-5S-208-12 (Simpson et al., 1985). The 416-bp DNA fragment 208-2 was cut out of pBS5S-208-2 by restriction with *Bam*H1 and *Eco*RV restriction enzymes. Histones H2–4 were prepared according to the method of Simon and Felsenfeld (1979). Reconstitution on 208-2 was carried out by salt dialysis in the caps of conventional reaction tubes (Eppendorf) by the method of Becker (Varga-Weisz et al., 1999). In a 60-μl reaction volume, a 3-μg fragment of 208-2 and a one- to fourfold amount of histones H2–4 were mixed in TE reconstitution buffer (10 mM Tris-HCl, 1 mM EDTA, 2 M NaCl, pH 7.5). The NaCl concentration in the buffer was lowered linearly from 1.5 M to 100 mM over 15 h, using a dialysis system consisting of two reservoirs and a pump. The samples were further dialyzed against the desired buffer for 2 h. Aliquots of the reconstituted material were analyzed on 1% agarose gels.

Analytical ultracentrifugation sedimentation velocity experiments

The oligonucleosome samples were centrifuged in a Beckman XL-A analytical ultracentrifuge at 40,000 rpm and scanned at 260 nm as fre-

quently as possible with the An-60Ti rotor (3-min intervals). The temperature was kept at 4°C, and the buffer was 10 mM Tris, 1 mM EDTA (pH 7.5), with 0 mM or 100 mM NaCl added. At least five sedimentation experiments were carried out with different preparations at both NaCl concentrations and at sample concentrations between 20 and 50 μg/ml. The sedimentation coefficient distributions were calculated with the program DCDT (Stafford, 1992; Stafford, 1994, 1997). The resulting $g(s^*)$ versus s^* curve is essentially of Gaussian shape, and the sedimentation coefficient s was determined from the maximum of the curve and corrected to standard conditions (20°C, H_2O) by using the relation

$$\frac{s_{20,w}}{s_{exp}} = \left(\frac{1-\bar{\nu}_{20,w}\cdot\rho_{20,w}}{1-\bar{\nu}_{T_{exp},buf}\cdot\rho_{T_{exp},buf}}\right)\cdot\left(\frac{\eta_{T_{exp},w}}{\eta_{20,w}}\right)\cdot\left(\frac{\eta_{T_{ref},buf}}{\eta_{T_{ref},w}}\right) \quad (1)$$

In this equation η is the viscosity and ρ is the density of the solution. The index exp refers to the experimental temperature, ref to a common reference temperature, w to water, and buf to the buffer solution used.

Literature values for the partial specific volume of chromatin and oligonucleosomes vary: a review by Durchschlag (1986) quotes values of $\bar{\nu} = 0.63\ldots 0.66$ cm^3/g, Hirai et al. (1988) found $\bar{\nu} = 0.663$ cm^3/g, while Butler and Thomas (1998) took the partial specific volume of chromatin as $\bar{\nu} = 0.69$ cm^3/g from Sperling (1976).

As shown below, the relationship between the sedimentation coefficient and the internucleosome distance is rather insensitive to the absolute value of $\bar{\nu}$. Here we used $\bar{\nu} = 0.67$ cm^3/g for the partial specific volume, which is between the cited values.

Simulation of sedimentation coefficients

The sedimentation coefficients of COS-7 and chicken erythrocyte di- and trinucleosomes were simulated with the program HYDRO (Garcia de la Torre et al., 1994). Nucleosomes were modeled as spherical beads with a molecular mass of 108,500 Da for the histone core octamer and 146 × 660 Da for the core DNA. To calculate the dependence of the sedimentation coefficient on the internucleosome distance, we follow a strategy similar to that applied by van Holde and Zlatanova (1996). First, the sedimentation coefficient of the nucleosome core particle was fixed to a known value; we used 11 S, as measured by Hirai et al. (1988). For a partial specific volume of $\bar{\nu} = 0.67$ cm^3/g and a molecular mass of 204,860 Da, the corresponding nucleosome radius is 55 Å. The DNA bead radius was chosen to be 15 Å, so that a linear array of spheres equals the volume of the cylindrical DNA with a hydrodynamic diameter of 24 Å (Hagerman and Zimm, 1981). The positions of the nucleosome and DNA beads were determined as follows. First, the distance between the nucleosome cores and the relative orientation of the nucleosome disks were fixed as input parameters. Second, the path of the linker DNA was calculated under the constraint that no kinks occurred at the exit points of the linker DNA. The resulting structure was visualized with the program RenderMan (Pixar Applications) on an Apple Macintosh computer. Third, the DNA path was divided into a linear array of spheres so that no overlap of two spheres occurred. The resulting positions of nucleosome and DNA spheres were written to a file in the input format of HYDRO. Finally, the sedimentation coefficient was calculated with HYDRO, using $\bar{\nu} = 0.67$ cm^3/g as above. Varying the value of $\bar{\nu}$ had no large effect on the computed sedimentation coefficient, as long as the nucleosome radius was adjusted in such a way that the correct sedimentation coefficient of the mononucleosome was obtained.

Small-angle neutron scattering experiments

Elastic neutron scattering experiments were performed at the D22 large-scale structure diffractometer at the Institut Laue-Langevin (ILL), Grenoble (for additional information see Buettner et al. (1997) and under the URL http://www.ill.fr/d22/D22.html). The sample cuvette (quartz, 1-mm light path for H_2O, 2-mm light path for D_2O, 7 × 10 mm^2 illuminated cross section; Hellma GmbH, Müllheim, Germany) was thermostatted at 8°C. The neutron wavelength was 8 Å, and the sample-detector distance was set to 8.0, 5.0, 4.0, 2.5, or 2.0 m to reach a momentum transfer q range of 0.008–0.3 Å^{-1}. The sample concentration was 1–1.7 mg/ml in TE buffer (10 mM Tris, 1 mM EDTA, pH 7.5, 0–100 mM NaCl). The NaCl concentration was varied by dialysis of the samples for at least 2 h against the desired buffer, with at least two buffer changes and a 1000-fold buffer volume. To check the reversibility of salt-dependent changes in the scattering curves, the samples were dialyzed from low to high salt and back. Data were collected for at least 1–2 h at each NaCl concentration, in H_2O as well as in D_2O. After radial integration the data were corrected for sample transmission. Electronic background and buffer scattering were subtracted. Fourier back-transformation was done with the indirect transformation method by Glatter (1977). We assumed a maximum distance in the dinucleosomes of 450 Å as an input parameter for the back-transformation software ITP. The Fourier-transformed scattering curve is the pair distance distribution function $p(r)$, indicating the probability of a certain distance r in the macromolecule:

$$p(r) = \frac{1}{2\pi^2}\int_{q_1}^{q_2} I(q)qr\sin(qr)\mathrm{d}q \quad (2)$$

$I(q)$ is the measured scattering intensity normalized to 1 after extrapolation to $q = 0$; $q = 4\pi g\cdot\sin(\theta/2)/\lambda$ is the scattering vector modulus, where λ is the neutron wavelength; and θ is the scattering angle. q_1 and q_2 are the minimal and maximal scattering vector moduli of the measured scattering curve.

Simulation of small-angle scattering curves

The small-angle scattering curves of COS-7 and chicken erythrocyte dinucleosomes were simulated as follows. First, as in the simulation of sedimentation coefficients, the dinucleosome structures were visualized as a function of internucleosomal distance, relative orientation, and linker DNA path. Second, the nucleosome core, core DNA, and linker DNA space of the dinucleosomes were filled randomly with ~1000 points. The actual number of points did not influence the predicted scattering curve above a lower limit of ~400 points per nucleosome. The protein core was modeled as a disk with diameter 65 Å and height 55 Å, and the DNA had a diameter of 24 Å, according to Dickerson et al. (1983), and was wrapped around the protein core in 1.7 turns. The ratio of the number of points in the protein core to the number of points in the core and linker DNA was chosen as a function of contrast:

$$I(q) \propto |b_m - b_s|^2 \quad (3)$$

$I(q)$ is the scattering intensity, and b_m and b_s are the scattering length densities of the macromolecule (DNA/protein) and the solvent (H_2O/D_2O). The mass was taken into account, calculating with 660 Da per base pair of DNA and 108,500 Da as total core histone mass per nucleosome. The coordinates of the points filling the dinucleosomes were then written to a file. We calculated the theoretical pair distance distributions $p(r)$ from the set of coordinates $\vec{r}_i$ and $\vec{r}_j$:

$$p(r) = \frac{1}{N^2}\sum_i\sum_j\begin{cases}1 & \text{if } \|\vec{r}_i - \vec{r}_j| - r| < \varepsilon \\ 0 & \text{otherwise}\end{cases} \quad (4)$$

The theoretical scattering curves were then calculated via transformation of $p(r)$ with the Debye Kernel:

$$I(q) = 4\pi\int_0^\infty p(r)\frac{\sin(qr)}{qr}\,\mathrm{d}r \quad (5)$$

RESULTS

Sample preparation and linker histone content

The DNA and protein composition of chicken erythrocyte oligonucleosomes are shown in Fig. 1, *a* and *b*, respectively. All samples contained the linker histones H1/H5. The COS-7 oligonucleosome composition is very similar (data not shown). The samples were also analyzed in 6% polyacrylamide gels (Fig. 1 *c*) to detect any nucleosome sliding, which occurs after several hours in a salt concentration higher than 100 mM NaCl and at room temperature, or any loss of nucleosomes. Sliding of nucleosomes on the DNA was found in only one sample; the scattering data were then discarded. The reconstituted samples were analyzed in 1% agarose gels (Fig. 1 *d*). Because an unknown number of histones bound to the reconstitution tube (conventional Eppendorf reaction tube), the mass ratio of histones to DNA in the reconstitution assay had to be titrated for every histone preparation. Depending on the mass ratio, the gel band shifted from 420 bp (no histones) to ~1400 bp (ratio histones:DNA = 3:1). Above a histone:DNA mass ratio of ~3, no further band shift was detected; therefore, only samples with the maximum band shift were used for the analytical ultracentrifugation experiments.

Analytical ultracentrifugation of dinucleosomes

The sedimentation coefficients of chicken erythrocyte, COS-7, and the reconstituted dinucleosomes were determined at 5 mM and at 100 mM NaCl. We repeated the experiments at different sample concentrations and with preparations of different days, but also with the same preparation and concentration at 5 and 100 mM NaCl. Typical distributions $g(s^*)$ are shown in Fig. 2. The shape of the distribution varies slightly from sample to sample because of slight changes in the MNase digestion time and the sucrose gradient fractions pooled. The sedimentation coefficient of chicken erythrocyte dinucleosomes increased from $s^* = 15.0 \pm 0.4$ S at 5 mM to $s^* = 17.5 \pm 0.6$ S at 100 mM salt, in agreement with the findings by Butler and

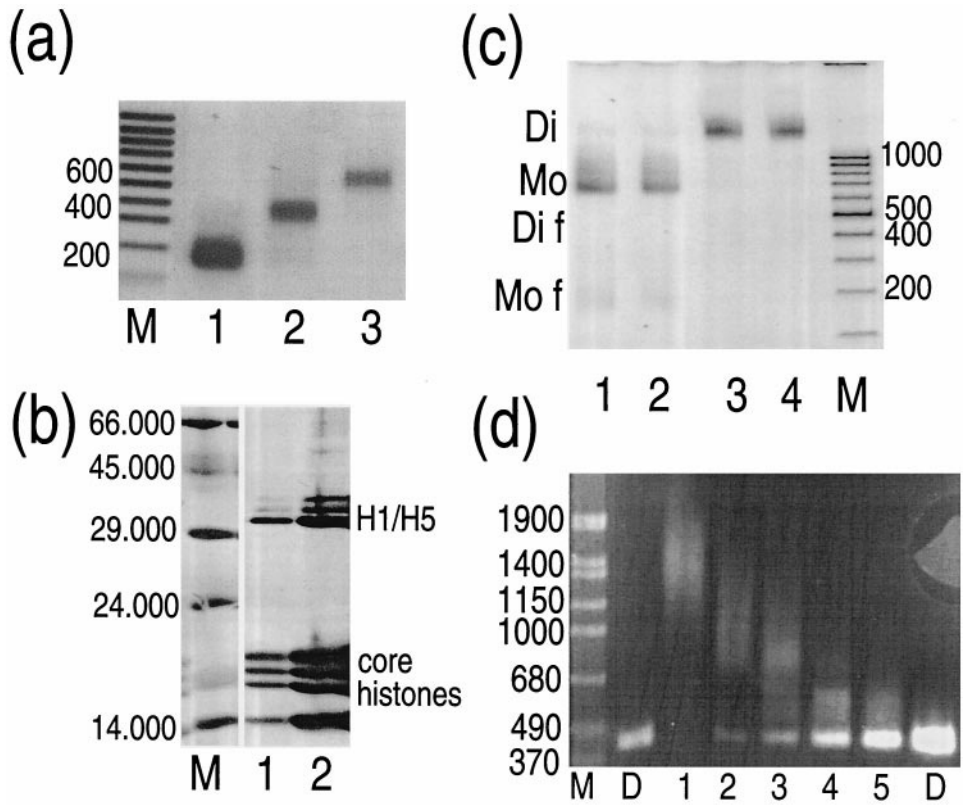

FIGURE 1 Composition of mono-, di-, and trinucleosomes, from chicken erythrocytes (*a* and *b*) and from COS-7 cells (*c*). (*a*) DNA analyzed in a 1% agarose gel. *Lane M*: Marker 100 base pair ladder (Fermentas). *Lanes 1–3*: Mono-, di-, and trinucleosomes. (*b*) Histone composition analyzed in an SDS/18% polyacrylamide gel. *Lanes 1* and *2*: Dinucleosomes from chicken erythrocyte chromatin, before and after sample concentration in VivaSpin concentration tubes. The protein marker is composed of different marker proteins; the molecular mass (in Da) is indicated. (*c*) Mono- (*lanes 1* and *2*; Mo) and dinucleosomes (*lanes 3* and *4*; Di) from COS-7 cells analyzed in 6% polyacrylamide gels. *Lane M*: Bioladder 100 (AGS). In lanes 1 and 2, very little mononucleosomal DNA (Mo f) is present between the 100-bp and 200-bp bands. In lanes 3 and 4, no free dinucleosomal DNA (Di f) or DNA with only one nucleosome can be detected. (*d*) Reconstituted dinucleosomes analyzed in a 1% agarose gel. M: BioSizer VI (AGS GmbH, Heidelberg). *Lane D*: DNA fragment 208-2. *Lanes 1–5*: Reconstituted dinucleosomes. Mass ratio histones:DNA = 3:1 (*lane 1*), 2.5:1 (*lane 2*), 2:1 (*lane 3*), 1.5:1 (*lane 4*), 1:1 (*lane 5*).

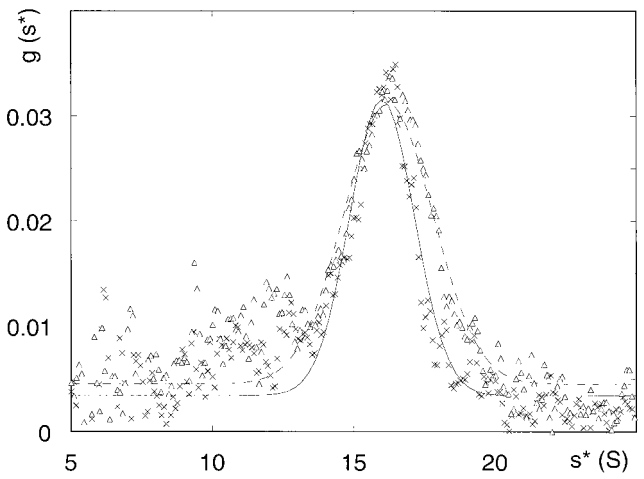

FIGURE 2 Measured distribution $g(s^*)$ of sedimentation coefficients s^* of COS-7 dinucleosomes, at two different Na^+ concentrations: 0 mM (×) and 100 mM (△), in TE buffer (10 mM Tris, 1 mM EDTA, pH 7.5).

Thomas (1998). The sedimentation coefficient of COS dinucleosomes changed from $s^* = 15.8 \pm 1.0$ S at 5 mM to $s^* = 16.7 \pm 1.2$ S at 100 mM salt (Fig. 3 *A*). Within experimental error these values are in agreement with the sedimentation behavior of rat liver dinucleosomes (Butler and Thomas, 1980). The sedimentation coefficient changes by less than 1 S. Yao et al. reported an increase in the translational diffusion coefficient D of chicken erythrocyte dinucleosomes as determined by dynamic light scattering, both with and without the linker histones (Yao et al., 1990, 1991), others did not find a salt-dependent change in D (Bednar et al., 1995). However, our findings are in line with the observation that chicken erythrocyte dinucleosomes compact with increasing salt (Butler and Thomas, 1998). The reconstituted dinucleosomes lacking the linker histone also showed an increase in s from $s = 13.5 \pm 1.0$ S at 5 mM NaCl to $s = 14.9 \pm 1.2$ S at 100 mM NaCl. These values agree well with those reported for H1-depleted dinucleosomes (Butler and Thomas, 1998) that are also shown in Fig. 3 *A*.

Simulation of sedimentation coefficients

The sedimentation coefficients of COS-7 and chicken erythrocyte di- and trinucleosomes were simulated with the program HYDRO (Garcia de la Torre et al., 1994). We started with the sedimentation coefficients of COS-7 dinucleosomes as a function of the internucleosomal distance d. The DNA repeat length was assumed to be 190 bp, the molecular mass 486,600 Da. With a straight linker DNA of 44 bp, d was 180 Å and the calculated sedimentation coefficient $s = 15.8$ S. Two possible conformations with extreme rotation are shown in Fig. 4 *A*. We found no difference in s between

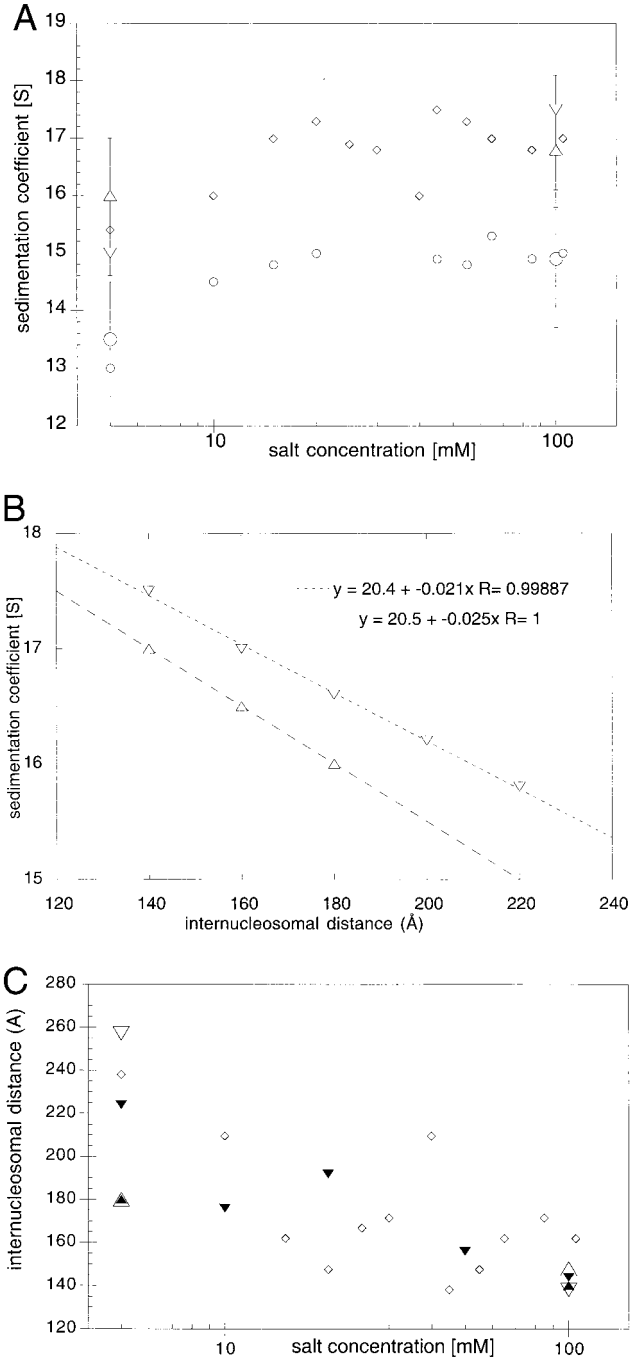

FIGURE 3 (*A*) Sedimentation coefficients of dinucleosome preparations versus salt concentration. Chicken (▽), COS (△), and reconstituted dinucleosomes (○) in comparison to the data of Butler and Thomas (1998) on H1-containing (◇) and H1-depleted (⊙) chicken dinucleosomes. (*B*) Simulated sedimentation coefficients for chicken (▽) and COS (△) dinucleosomes versus internucleosomal distance. (*C*) Internucleosomal distance versus salt concentration as computed from the sedimentation coefficients in *A* and *B* (chicken (▽), COS (△) dinucleosomes, and data of Butler and Thomas (1998) for H1-containing chicken dinucleosomes (◇)) and from the neutron scattering data (Fig. 10) on chicken (▼) and COS (▲) dinucleosomes.

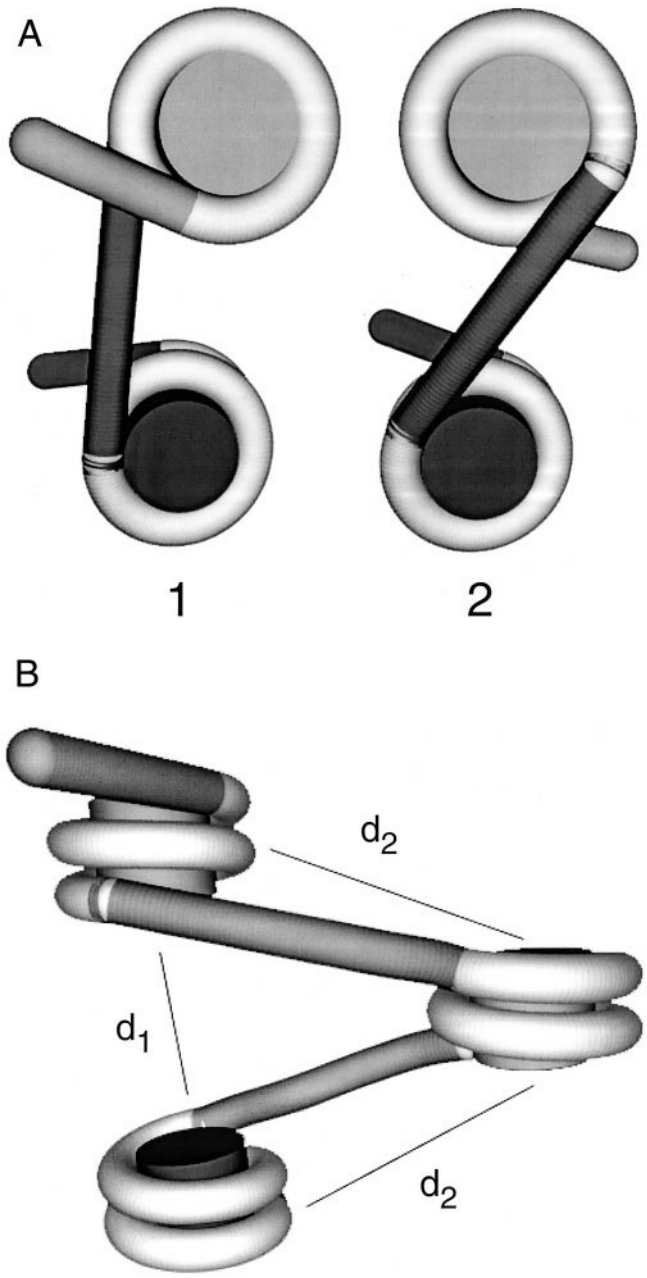

FIGURE 4 (*A*) Simulated structures of COS dinucleosomes, with two extremes of rotational alignment. Both structures yielded a simulated sedimentation coefficient of s = 16.6 S. (*B*) Simulated structure of chicken erythrocyte trinucleosomes. d_1 is the distance between opposing and d_2 that between neighboring nucleosomes.

these two and other possible rotational alignments. When d decreases to 140 Å, the sedimentation coefficient increases to s = 16.7 S (Fig. 3 *B*).

Second, we simulated the sedimentation coefficients of chicken erythrocyte dinucleosomes. The DNA repeat length was assumed to be 210 bp, the molecular mass 513,200 Da (van Holde and Zlatanova, 1996). The simulated values as a function of d are shown in Fig. 3 *B*. A linear fit to the data enabled us to convert the measured sedimentation coefficients into an internucleosome distance d. For chicken erythrocyte dinucleosomes, we obtained a linear regression of d (Å) = (20.4 − s (S))/0.021 and, for COS dinucleosomes, d (Å) = (20.5 − s (S))/0.025. The calculated distances are shown in Fig. 3 *C* as a function of the salt concentration. For chicken erythrocyte dinucleosomes, d decreases strongly from ~220–230 Å to ~120–130 Å between 5 and 100 mM NaCl. The data by Butler and Thomas (1998) indicate that the largest decrease occurs between 5 and 20 mM salt. The COS dinucleosomes show a smaller decrease from 170 Å at 5 mM to 140 Å at 100 mM NaCl. Thus the sedimentation data do argue in favor of a salt-dependent change in the internucleosomal distance d.

Third, we simulated the sedimentation coefficients of chicken erythrocyte trinucleosomes. The DNA repeat length was 210 bp and the molecular mass 769,800 Da. The distances d_1 and d_2 (see Fig. 4 *B*) between the nucleosomes were varied in two ways. The distance d_2 between adjacent nucleosomes was kept constant and d_1 was reduced, or both distances were reduced homogeneously, starting from d_1 = d_2 = 220 Å. The calculated values are shown in Table 1. For both methods of compaction, the simulated values agree with the measured data of Butler and Thomas (1998), who found an increase in s from 19 S at 5 mM to 21 S at 20 mM NaCl and at higher salt concentrations. In the case of homogeneous compaction, the values are compatible up to a distance between the nucleosomes of ~150 Å. Thus, from the sedimentation experiments and simulations alone, the mechanism of compaction of the trinucleosomes cannot be deduced unambiguously.

Neutron small-angle scattering experiments

Elastic neutron scattering data were collected on chicken erythrocyte and COS-7 di- and trinucleosomes, both in H_2O and in D_2O, at NaCl concentrations between 5 and 100 mM. In general, we used the D_2O data for a more precise internucleosomal distance determination, because the contrast of the protein versus background is higher than in H_2O. However, several experiments were done in H_2O to exclude

TABLE 1 Simulated sedimentation coefficients of chicken erythrocyte trinucleosomes

d_1 (Å)	d_2 (Å)	s (S)
200	220	19.2
180	220	19.6
160	220	20.0
140	220	20.5
120	220	21.0
180	180	20.0
160	160	21.0
140	140	22.2
120	120	23.6

The distances d_1 and d_2 are defined in Fig. 4 *B*.

artifacts. Figs. 5 and 6 show the measured scattering intensity of chicken erythrocyte and COS-7 dinucleosomes in D_2O at 5 and at 100 mM NaCl. For both molecules, the scattering intensity at a scattering vector of $q \approx 0.04$ Å^{-1} decreases with increasing salt concentration from 5 to 100 mM NaCl. The effect is reversible and also present in H_2O but less visible because of the higher noise (data not shown).

Because the scattering intensity of nucleosomes in D_2O is dominated by scattering from proteins (i.e., histones), the salt-dependent change in the scattering intensity could reflect a change in the internucleosomal distance d. We therefore calculated theoretical scattering curves of dinucleosomes for different distances d as shown in Fig. 7. The model was as in Fig. 4 *A*, from which a set of coordinates was calculated as described above. Fig. 8 shows the x and y components of a set of coordinates for $d = 220$ Å (*top*).

With decreasing d, an undulation in the simulated scattering curves present at about $q = 0.03$ Å^{-1} shifts to higher q values and disappears below $d = 140$ Å. We multiplied the simulated scattering curves by an arbitrary factor to fit them to the measured curves. The measured data for chicken erythrocyte dinucleosomes at 5 and 100 mM NaCl are shown together with the simulated curve at $d = 220$ Å in Fig. 9. The simulated curve and the measured data at 5 mM have the same undulation present at $q = 0.03$ Å^{-1}; however, its amplitude is larger in the simulated curve. The reason for this might be the fact that the measured data are smeared because the distribution of nucleosomal distances in the dinucleosome is not a sharp peak but a broad Gaussian. We therefore added 20% random noise to the x, y, and z components of the coordinates of the scattering, as shown in Fig. 8 (*center* and *bottom*). From these modified sets of coordinates, we calculated the modified scattering curves shown in Fig. 9, which contain a less pronounced undulation. The modified simulated scattering curves fit the experimental data well under the assumption that the nucleosomal distance d decreases from 220 Å at 5 mM to 140–150 Å at 100 mM NaCl for the chicken erythrocyte dinucleosomes and from 180 Å at 5 mM to 140 Å at 100 mM for the COS dinucleosomes.

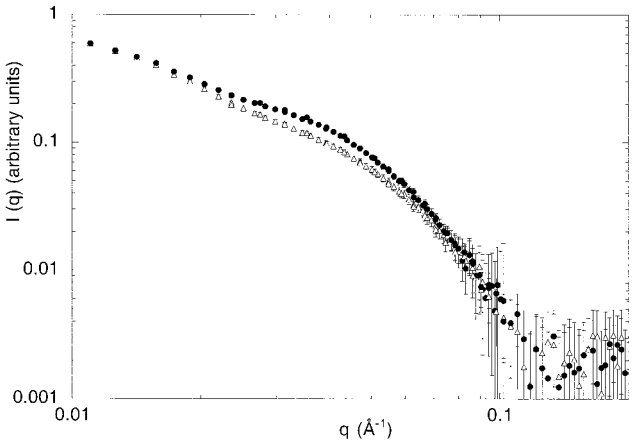

FIGURE 6 Measured neutron scattering intensity $I(q)$ of COS dinucleosomes, in D_2O, Tris buffer, at two different Na^+ concentrations: 5 mM (●) and 100 mM (△).

In H_2O, we also collected scattering data at 10, 20, and 50 mM NaCl. A Fourier back-transformation of the scattering curves with the program ITP yielded the pair distance distributions $p(r)$, as shown in Fig. 10 for chicken erythrocyte dinucleosomes. The curves have a maximum at 55 Å, which is the radius of a nucleosome. The curves at 10 mM and 20 mM NaCl have a secondary maximum at $r = 200$ Å, indicating an internucleosomal distance of $d = 200$ Å at this salt concentration. At 50 and 100 mM NaCl, the maximum disappears and the fraction of distances in the range 100–150 Å increases, which is probably due to the decrease in

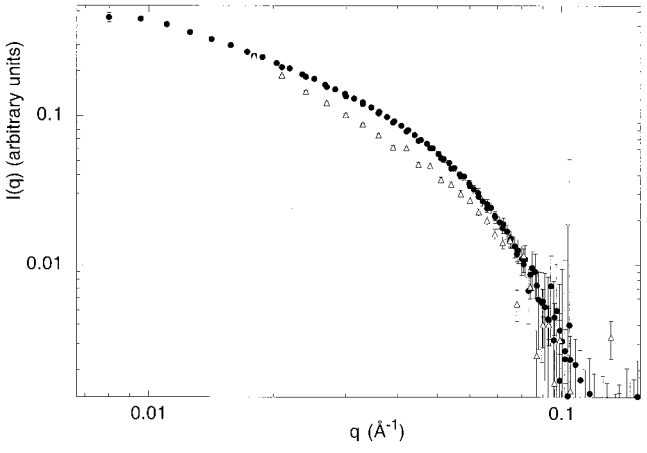

FIGURE 5 Measured neutron scattering intensity $I(q)$ of chicken erythrocyte dinucleosomes, in D_2O, Tris buffer, at two different Na^+ concentrations: 5 mM (●) and 100 mM (△).

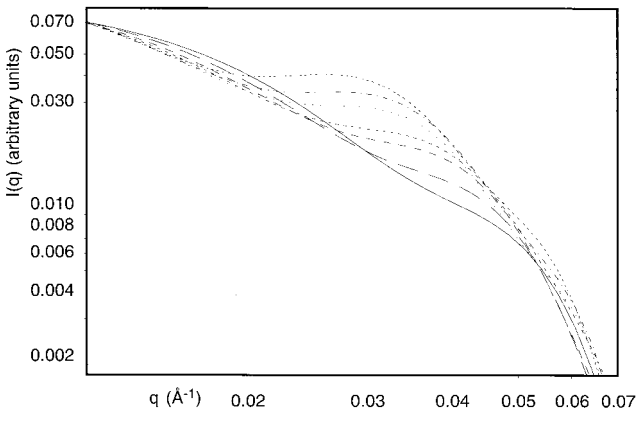

FIGURE 7 Simulated scattering curves of dinucleosomes as a function of the internucleosomal distance d: 120 Å (——), 140 Å (— —), 160 Å (— —), 180 Å (— — —), 200 Å (- - - - - -), 220 Å (- - - - - -), 240 Å (- - - - - - - - -).

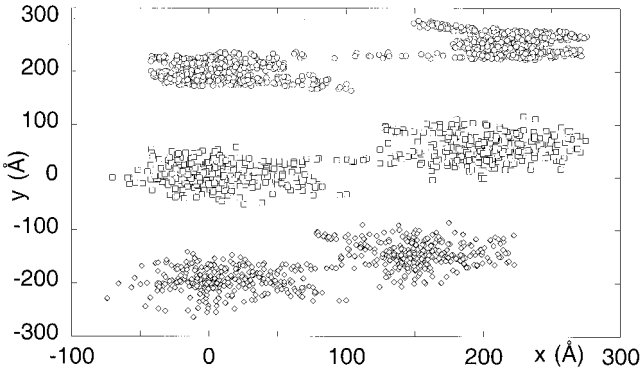

FIGURE 8 x versus y component of the space coordinates of the dinucleosome model. The space coordinates were calculated by randomly filling the models as shown in Fig. 3 *A*, with the number of points chosen according to the relative scattering intensity of DNA and proteins in the surrounding solvent H_2O/D_2O. The scattering curves in Fig. 7 were calculated from the model as shown at the top. *Center* and *bottom*: 20% random noise was added to the x, y, and z coordinates of the exact model. *Top* and *center*: dinucleosome distance $d = 220$ Å. *Bottom*: $d = 150$ Å.

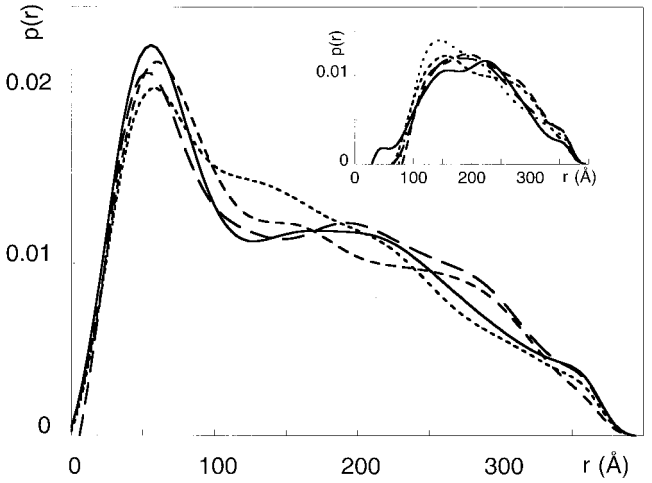

FIGURE 10 Pair distance distribution function $p(r)$ of chicken erythrocyte dinucleosomes in H_2O at 10 mM (——), 20 mM (– – –), 50 mM (— — —), and 100 mM (- - -) NaCl. The $p(r)$ function was calculated by back-transformation of the measured scattering curves by use of the program ITP. *Inset*: The same distributions, from which a Gaussian corresponding to the mononucleosomal distance distribution function was subtracted, characterizing the internucleosomal pair distance distribution function.

the internucleosomal distance d as pointed out above. The main change in d appears in the range 50–100 mM NaCl. To highlight the changes in the internucleosomal distance, we fitted a Gaussian distribution to the $p(r)$ function of mononucleosomes (data not shown). This Gaussian was subtracted by the dinucleosome $p(r)$ functions from Fig. 10. The resulting distribution functions are shown in the inset in Fig. 10. A maximum at ~210 Å at 5 mM shifts to ~140 Å at 100 mM. The positions of the maxima for both chicken erythrocyte and COS dinucleosomes are compared with the sedimentation experiment results in Fig. 3 *C*. Both methods argue in favor of a salt-dependent compaction. The sedimentation results by Butler and Thomas (1998) show the largest change in the sedimentation coefficient between 5 and 20 mM NaCl, whereas our neutron data suggest a more continuous effect.

To study the folding process of longer oligonucleosomes, we collected scattering data on chicken erythrocyte and COS trinucleosomes in H_2O. The scattering curves of chicken erythrocyte trinucleosomes have a slight but significant salt dependence, as can be seen in Fig. 11. The curves coincide between 0 and 20 mM NaCl (only the 0 and 100 mM NaCl data are shown in Fig. 11), whereas at 100 mM NaCl a decrease in the scattering intensity at $q \approx 0.03$ Å^{-1}

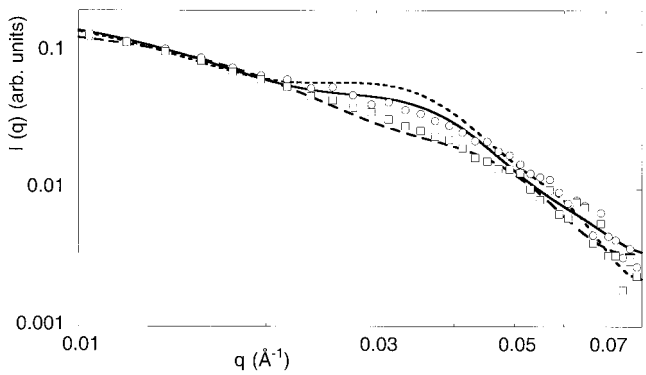

FIGURE 9 Measured and simulated scattering curves of chicken erythrocyte dinucleosomes in D_2O, Tris buffer, 5 mM (○) and 100 mM (□) NaCl. The simulated scattering curves are calculated from the model as shown in Fig. 8. The exact structure (*top* in Fig. 8) yields the upper scattering curve (- - - - -), while the structures with 20% random noise yield the lower curves, with $d = 220$ Å (——) and $d = 140$ Å (– – –).

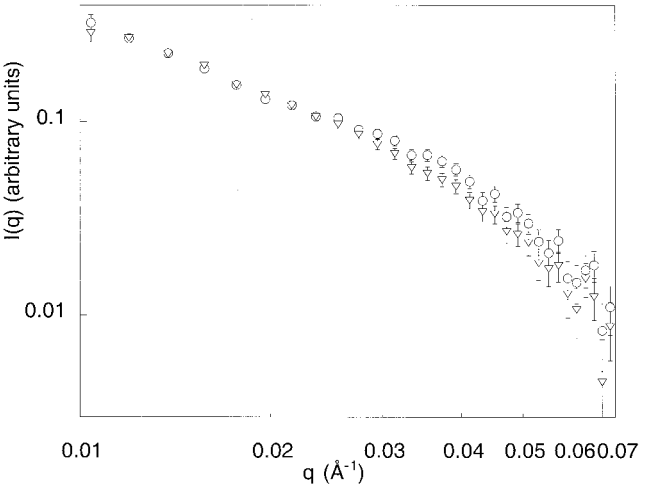

FIGURE 11 Measured neutron scattering intensity $I(q)$ of chicken erythrocyte trinucleosomes, in H_2O, Tris buffer, at two different Na^+ concentrations: 5 mM (○) and 100 mM (▽).

is clearly visible. As above, theoretical scattering curves were calculated from simulated structures (data not shown). The theoretical curves again contained sharper features than the measured data, indicating that the trinucleosomes are in an ensemble of possible conformations with similar free energy. A Fourier back-transformation of the scattering curves by use of the ITP program yielded the pair distance distribution functions $p(r)$ as shown in Fig. 12. A very pronounced maximum at 210 Å, present between 5 and 20 mM NaCl, disappears at 50 mM. The maximum is less pronounced for the COS trinucleosomes (Fig. 13) but is still present at $r = 180$ Å, and the salt-dependent change in $p(r)$ is very similar. It is very likely that the maximum is the distance between adjacent nucleosomes, which probably stays constant at ~210 Å for the chicken erythrocyte trinucleosomes and at 180 Å for the COS dinucleosomes up to a salt concentration of ~20 mM. The sedimentation experiments by Butler and Thomas (1998) favored a compaction in this salt concentration range; thus the trinucleosomes are probably compacted by a change in the distance d_1 as shown in Fig. 4 *B*. This mechanism has been suggested by van Holde and Zlatanova (1996). At a salt concentration of ~50 mM, the fraction of distances in $p(r)$ at $r = 120$ Å strongly increases for both types of trinucleosomes, which is very similar to the behavior of the dinucleosomes.

We propose that the compaction of the trinucleosomes might proceed through two different mechanisms, depending on the salt concentration. Between 0 and 20 mM NaCl, the internucleosomal distance between adjacent nucleosomes remains constant, whereas the angle at the central nucleosome between the two outer nucleosomes decreases. At 50 mM and higher salt concentrations, the distance between adjacent nucleosomes decreases. The sedimentation coefficient of 21 S for chicken erythrocyte trinucleosomes at 100 mM NaCl (Butler and Thomas, 1998) sets a lower limit to the distance between adjacent nucleosomes of ~150 Å. The sedimentation coefficient would have been higher if the distance had been smaller. We repeated the sedimentation experiment on our trinucleosome sample and found $s = 21.3 \pm 0.8$ S, in agreement with Butler and Thomas (1998).

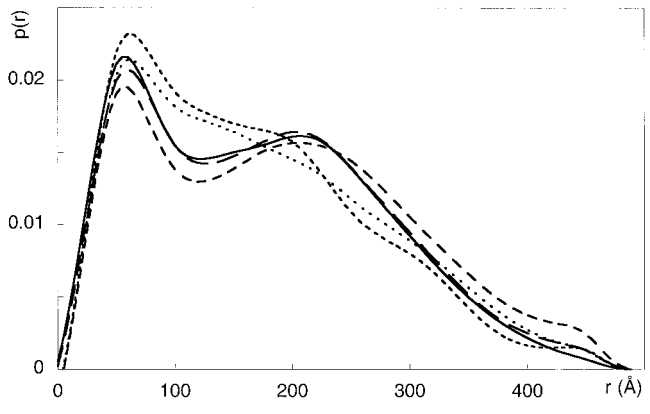

FIGURE 12 Pair distance distribution function $p(r)$ of chicken erythrocyte trinucleosomes, calculated from the scattering curves in H_2O as shown in Fig. 11 at 5 mM (——), 10 mM (— — —), 20 mM (— — —), 50 mM (- - - - - - -), and 100 mM (- - - - -) NaCl. The $p(r)$ function was calculated by back-transformation of the measured scattering curves by use of the program ITP.

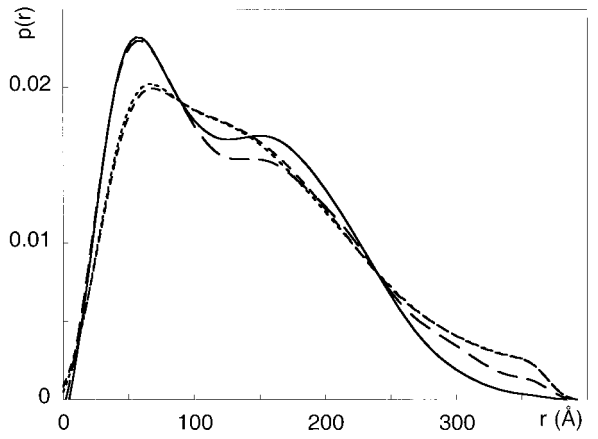

FIGURE 13 Pair distance distribution function $p(r)$ of COS trinucleosomes, calculated from the scattering curves in H_2O at 10 mM (——), 20 mM (— — —), 50 mM (— — —), and 100 mM (- - - - -) NaCl.

DISCUSSION

From our neutron small-angle scattering and sedimentation studies on native di- and trinucleosomes, as well as from the sedimentation data on reconstituted dinucleosomes, the consensus picture emerges that in all cases the structure compacts with a change in the salt concentration from 5 to 100 mM NaCl. This can be interpreted as a salt-induced decrease in the internucleosomal distance. While similar compaction effects have been reported by other groups (Yao et al., 1990, 1991; Butler and Thomas, 1998), this is to our knowledge the first time that sedimentation and neutron scattering data on the same set of nucleosome preparations could be correlated with predictions from a hydrodynamic model.

The distance of ~220 Å for chicken erythrocyte dinucleosomes in low-salt buffer is compatible with the assumption that the linker DNA of 62 bp is fully extended (van Holde and Zlatanova, 1996). This distance decreases to ~140–150 Å at high salt. These changes can be interpreted in several different ways. First, the linker DNA between the nucleosomes could assume a bent or kinked conformation. This assumption is required for the solenoid model, in which the DNA follows a continuous spiral path around and between successive histone cores. The drawback of this hypothesis is that it requires very tight bending of the DNA. The energy required to bend a piece of DNA of length $L =$ 80 bp with a persistence length L_p of 50 nm = 147 bp

(Hagerman, 1988) into a full circle ($\theta = 360°$) is $E_B = (k_BT/2)\theta^2(L_P/L) = 36\ k_BT$. Bending 50 bp of linker DNA around the same radius would require 5/8 of this energy, or 23 k_BT = 56 kJ/mol. While it is possible to gain such an amount of energy from interactions of the linker DNA with the histone proteins, models in which the DNA is not highly bent have the advantage that no such energy input is required.

Second, the bend could also occur at the nucleosome "stem," the structure formed by the linker DNA and the linker histone that has been observed in cryoelectron microscopy images (Hamiche et al., 1996; Bednar et al., 1998). In this case, the bend would have to be very sharp, larger than 90°, to account for the large distance change of ~70 Å in the chicken erythrocyte dinucleosomes. While this possibility cannot be ruled out either, because associated proteins such as HMG1/2 might induce a bend in the DNA, it would not explain our observation that reconstituted nucleosomes without linker histones and other proteins also show a salt-induced compaction.

Finally, an intermediate situation that could explain the distance decrease without assuming a homogeneously bent linker DNA would be an increased wrapping of part of the linker DNA around the histone core. A distance change of 70 Å corresponds to ~20 bp, and 40 Å to 12 bp, assuming a DNA length of 3.4 Å/bp. The additional 20 bp could be bound to the histone octamer in 1.94 instead of 1.7 turns of the DNA around the protein core as shown in Fig. 14. This would mean that in the case of chicken erythrocyte chromatin, ~166 instead of 146 bp would be bound to the histone octamer. It is well established that in the presence of the linker histone, 170 bp is protected against micrococcal nuclease (MNase) attack. Even in digests of reconstituted chromatin lacking the linker histones, the 170 bp is also protected at higher salt (van Holde, 1989, p. 270, and references therein). As pointed out in the description of the nucleosome core structure by Luger et al. (1997), only 121 bp of the 146 bp core DNA is bound to the histone octamer via hydrogen bonds. The remaining 25 bp of the DNA used in the crystallographic study is probably contacted by the N-terminal histone tails of the core histones, but additional base pairs could also be contacted by the histone tails.

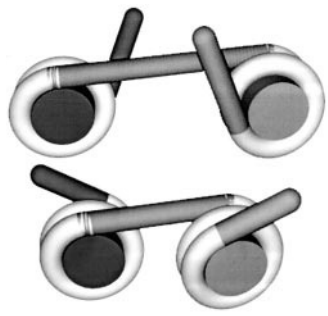

FIGURE 14 Possible compaction mechanism of chicken erythrocyte dinucleosomes. The effective length of the linker DNA is reduced because the DNA is wrapped around the histone core in 1.94 turns (*bottom*) instead of 1.7 turns (*top*).

We prefer this latter interpretation because an "opening" of the nucleosome structure from the linker DNA ends constitutes a very plausible mechanism for changing the degree of folding of the chromatin fiber. Because acetylation of the histone tails is involved in transcriptional regulation, a possible mechanism of the opening of the chromatin structure during transcription could be a release of base pairs from the histone octamer due to acetylation of the histone tails (Chahal et al., 1980; Fletcher and Hansen, 1996; Luger and Richmond, 1998; Usachenko et al., 1996). In the paper by Usachenko et al. (1996), it is demonstrated that an altered nucleosome conformation present in unfolded linker-histone-depleted chromatin might occur during chromatin activation and that it might be caused by the stretching of linker DNA during chromatin unfolding.

The data of this study on their own cannot yet indicate decisively whether the solenoid or other models of the 30-nm chromatin fiber are correct. From our neutron scattering data and the sedimentation data by Butler and Thomas (1998), the shortening of dinucleosome linker DNA would be consistent with both solenoidal and straight linker models.

However, the compaction of trinucleosomes can be used to interpret recent data from scanning force microscopy (Leuba et al., 1998a,b) and cryoelectron microscopy (Bednar et al., 1998). As pointed out above, our data suggest a two-step compaction process of the trinucleosomes. Between 0 and 20 mM NaCl, the linker DNA remains extended, and the angle at the central nucleosome formed by the outer nucleosomes decreases. This could explain why the nucleosomes are clearly separated in the microscopy images and why the fiber seems to condense in an accordion-like manner. At higher salt concentration, the distance between the adjacent nucleosomes decreases and the fiber becomes more compact by an approach of the neighboring nucleosomes. This might be why already in 60 mM NaCl the fiber becomes very dense in the microscopy images and individual nucleosomes can hardly be separated in the images.

Our measured distance of ~140–150 Å between nucleosomes in 100 mM salt corresponds well with the 150-Å nucleosome distance in longer chromatin fibers fixed with glutaraldehyde and imaged by scanning force microscopy (Zlatanova et al., 1998). In contrast, unfixed fibers on glass showed distances of ~200 Å, similar to the low-salt distance of nucleosomes reported here. Thus the glutaraldehyde fixation process might preserve the fiber in its native state. Similarly, dinucleosomes fixed with glutaraldehyde in conventional electron microscopy have an average nucleosome distance of 150 Å, whereas frozen-hydrated dinucleosomes imaged by cryoelectron microscopy show a distance of 300 Å between the two nucleosomes (Bednar et al., 1995).

While our results rule out neither the solenoid nor the random zigzag model of the chromatin fiber, they can help to interpret microscopic and biochemical data. However,

further measurements with longer fibers will be necessary to arrive at a decision about the fiber structure in its compact state at physiological salt concentrations.

We are very grateful to Gabriele Müller and Katalin Fejes Tóth for technical assistance in tissue culture and preparation of the oligonucleosomes. We gratefully acknowledge the support from the Institute Laue-Langevin, particularly the grant of measuring time on the instrument D22. We thank Nathalie Brun and Thomas Weidemann for help with the preparations and the neutron scattering experiments.

Parts of this work were supported by German Ministry of Science and Technology (BMBF) grant 01KW9620 to JL.

REFERENCES

Bednar, J., R. A. Horowitz, J. Dubochet, and C. L. Woodcock. 1995. Chromatin conformation and salt-induced compaction: three-dimensional structural information from cryoelectron microscopy. *J. Cell Biol.* 131:1365–1376.

Bednar, J., R. A. Horowitz, S. A. Grigoryev, L. M. Carruthers, J. C. Hansen, A. J. Koster, and C. L. Woodcock. 1998. Nucleosomes, linker DNA, and linker histone form a unique structural motif that directs the higher-order folding and compaction of chromatin. *Proc. Natl. Acad. Sci. USA.* 95:14173–14178.

Buettner, H. G., E. Lelievre-Berna, and F. Pinet, editors. 1997. Yellow Book: Guide to Neutron Research Facilities at the ILL. Institut Laue-Langevin, Grenoble.

Butler, P. J., and J. O. Thomas. 1980. Changes in chromatin folding in solution. *J Mol. Biol.* 140:505–529.

Butler, P. J., and J. O. Thomas. 1998. Dinucleosomes show compaction by ionic strength, consistent with bending of linker DNA. *J. Mol. Biol.* 281:401–407.

Chahal, S. S., H. R. Matthews, and E. M. Bradbury. 1980. Acetylation of histone H4 and its role in chromatin structure and function. *Nature.* 287: 76–79.

Dickerson, R. E., H. R. Drew, B. N. Conner, M. L. Kopka, and P. E. Pjura. 1983. Helix geometry and hydration in A-DNA, B-DNA and Z-DNA. *Cold Spring Harb. Symp. Quant. Biol.* 47:13–24.

Dong, F., and K. E. van Holde. 1991. Nucleosome positioning is determined by the (H3–H4)2 tetramer. *Proc. Natl. Acad. Sci. USA.* 88: 10596–10600.

Durchschlag, H. 1986. Specific volumes of biological macromolecules and some other molecules of biological interest. *In* Thermodynamic Data for Biochemistry and Biotechnology. H.-J. Hinz, editor. Springer-Verlag, Berlin.45–128.

Finch, J. T., and A. Klug. 1976. Solenoidal model for superstructure in chromatin. *Proc. Natl. Acad. Sci. USA.* 73:1897–1901.

Fletcher, T. M., and J. C. Hansen. 1996. The nucleosomal array: structure/function relationships. *Crit. Rev. Eukaryot. Gene Exp.* 6:149–188.

Garcia de la Torre, J., S. Navarro, M. C. López Martínez, F. G. Díaz, and J. J. López Cascales. 1994. HYDRO: a computer software for the prediction of hydrodynamic properties of macromolecules. *Biophys. J.* 67:530–531.

Gerchman, S. E., and V. Ramakrishnan. 1987. Chromatin higher-order structure studied by neutron scattering and scanning transmission electron microscopy. *Proc. Natl. Acad. Sci. USA.* 84:7802–7806.

Glatter, O. 1977. Data evaluation in small angle scattering: calculation of the radial electron density distribution by means of indirect Fourier transformation. *Acta Physica Austriaca.* 47:83–102.

Godde, J. S., and J. Widom. 1992. Chromatin structure of *Schizosaccharomyces pombe*. A nucleosome repeat length that is shorter than the chromatosomal DNA length. *J. Mol. Biol.* 226:1009–1025.

Graziano, V., S. E. Gerchman, D. K. Schneider, and V. Ramakrishnan. 1994. Histone H1 is located in the interior of the chromatin 30-nm filament. *Nature.* 368:351–354.

Hagerman, P. J. 1988. Flexibility of DNA. *Annu. Rev. Biophys. Biophys. Chem.* 17:265–286.

Hagerman, P. J., and B. H. Zimm. 1981. Monte Carlo approach to the analysis of the rotational diffusion of wormlike chains. *Biopolymers.* 20:1481–1502.

Hamicher, A., P. Schultz, V. Ramakrishnan, P. Oudet, and A. Prunell. 1996. Linker histone-dependent DNA structure in linear mononucleosomes. *J. Mol. Biol.* 257:30–42.

Hirai, M., N. Niimura, M. Zama, K. Mita, S. Ichimura, F. Tokunaga, and Y. Ishikawa. 1988. Interparticle interactions and structural changes of nucleosome core particles in low-salt solution. *Biochemistry.* 27:7924–7931.

Leuba, S. H., C. Bustamante, K. van Holde, and J. Zlatanova. 1998a. Linker histone tails and N-tails of histone H3 are redundant: scanning force microscopy studies of reconstituted fibers. *Biophys. J.* 74: 2830–2839.

Leuba, S. H., C. Bustamante, J. Zlatanova, and K. van Holde. 1998b. Contributions of linker histones and histone H3 to chromatin structure: scanning force microscopy studies on trypsinized fibers. *Biophys. J.* 74:2823–2829.

Luger, K., A. W. Mäder, R. K. Richmond, D. F. Sargent, and T. J. Richmond. 1997. Crystal structure of the nucleosome core particle at 2.8 Å resolution. *Nature.* 389:251–260.

Luger, K., and T. J. Richmond. 1998. The histone tails of the nucleosome. *Curr. Opin. Genet. Dev.* 8:140–146.

Rydberg, B., W. R. Holley, I. S. Mian, and A. Chatterjee. 1998. Chromatin conformation in living cells: support for a zigzag model of the 30 nm chromatin fiber. *J. Mol. Biol.* 284:71–84.

Simon, R. H., and G. Felsenfeld. 1979. A new procedure for purifying histone pairs H2A + H2B and H3 + H4 from chromatin using hydroxylapatite. *Nucleic Acids Res.* 6:689–696.

Simpson, R. T., F. Thoma, and J. M. Brubaker. 1985. Chromatin reconstituted from tandemly repeated cloned DNA fragments and core histones: a model system for study of higher order structure. *Cell.* 42:799–808.

Sperling, L. 1976. The mass per unit length of chromatin by low-angle x-ray scattering. *FEBS Lett.* 64:89–91.

Stafford, W. F. 1992. Methods for obtaining sedimentation coefficient distributions. *In* Analytical Ultracentrifugation in Biochemistry and Polymer Science. S. E. Harding, A. J. Rowe, and J. Horton, editors. Royal Society of Chemistry, Cambridge. 359–393.

Stafford, W. F. 1994. Boundary analysis in sedimentation velocity experiments. *Methods Enzymol.* 240:478–501.

Stafford, W. F. 1997. Sedimentation velocity spins a new weave for an old fabric. *Curr. Opin. Biotechnol.* 8:14–24.

Usachenko, S. I., I. M. Gavin, and S. G. Bavykin. 1996. Alterations in nucleosome core structure in linker histone-depleted chromatin. *J. Biol. Chem.* 271:3831–3836.

van Holde, K. E. 1989. Chromatin. Springer-Verlag, Heidelberg.

van Holde, K., and J. Zlatanova. 1995. Chromatin higher order structure: chasing a mirage? *J. Biol. Chem.* 270:8373–8376.

van Holde, K., and J. Zlatanova. 1996. What determines the folding of the chromatin fiber. *Proc. Natl. Acad. Sci. USA.* 93:10548–10555.

Varga-Weisz, P. D., E. J. Bonte, and P. B. Becker. 1999. Analysis of modulators of chromatin structure in *Drosophila*. *Methods Enzymol.* 304:742–757.

Widom, J. 1998. Structure, dynamics, and function of chromatin in vitro. *Annu. Rev. Biophys. Biomol. Struct.* 27:285–327.

Woodcock, C. L., and R. A. Horowitz. 1995. Chromatin organization reviewed. *Trends Cell Biol.* 5:272–277.

Yao, J., P. T. Lowary, and J. Widom. 1990. Direct detection of linker DNA bending in defined-length oligomers of chromatin. *Proc. Natl. Acad. Sci. USA.* 87:7603–7607.

Yao, J., P. T. Lowary, and J. Widom. 1991. Linker DNA bending induced by the core histones of chromatin. *Biochemistry.* 30:8408–8414.

Zlatanova, J., S. H. Leuba, and K. van Holde. 1998. Chromatin fiber structure: morphology, molecular determinants, structural transitions. *Biophys. J.* 74:2554–2566.